Pattern Recognition 99 (2020) 107064

Contents lists available at ScienceDirect

Pattern Recognition

journal homepage: www.elsevier.com/locate/patcog

Tooth morphometry using quasi-conformal theory

Gary P.T. Choi[a], Hei Long Chan[b], Robin Yong[c], Sarbin Ranjitkar[c], Alan Brook[c], Grant Townsend[c], Ke Chen[d], Lok Ming Lui[b,*]

[a] John A. Paulson School of Engineering and Applied Sciences, Harvard University, USA
[b] Department of Mathematics, The Chinese University of Hong Kong, Hong Kong China
[c] Adelaide Dental School, The University of Adelaide, Australia
[d] Department of Mathematical Sciences, The University of Liverpool, United Kingdom

ARTICLE INFO

Article history:
Received 7 January 2019
Revised 3 September 2019
Accepted 23 September 2019
Available online 26 September 2019

Keywords:
Tooth morphometry
Quasi-conformal theory
Shape analysis
Teichmüller map
Ancestry
Sexual dimorphism
Classification

ABSTRACT

Shape analysis is important in anthropology, bioarchaeology and forensic science for interpreting useful information from human remains. In particular, teeth are morphologically stable and hence well-suited for shape analysis. In this work, we propose a framework for tooth morphometry using quasi-conformal theory. Landmark-matching Teichmüller maps are used for establishing a 1-1 correspondence between tooth surfaces with prescribed anatomical landmarks. Then, a quasi-conformal statistical shape analysis model based on the Teichmüller mapping results is proposed for building a tooth classification scheme. We deploy our framework on a dataset of human premolars to analyze the tooth shape variation among genders and ancestries. Experimental results show that our method achieves much higher classification accuracy with respect to both gender and ancestry when compared to the existing methods. Furthermore, our model reveals the underlying tooth shape difference between different genders and ancestries in terms of the local geometric distortion and curvatures. In particular, our experiment suggests that the shape difference between genders is mostly captured by the conformal distortion but not the curvatures, while that between ancestries is captured by both of them.

1. Introduction

Shape analysis and classification is an important topic in pattern recognition [1,2]. The use of computer technology in medicine and biology dates back to the seminal works by Ledley et al. [3–5] in the1950's and60's, which formed the foundation of modern computerized biomedical analysis. To detect patterns from shapes, landmarks have been widely used [6–8]. By comparing the landmark positions of different shapes, one can have a better understanding of their difference. Therefore, it is necessary to have an effective method for landmark-based shape matching. Furthermore, a method for detecting and extracting the underlying geometric variation of the shapes is needed for classifying them.

Geometric morphometrics (GM) aims at analyzing biological forms using Cartesian geometric coordinates [9]. The Procrustes superimposition method [10] aligns and compares two shapes by rescaling, translating and rotating two sets of landmarks defined on them to a common size and position. The thin plate spline (TPS) method [11] finds a non-rigid transformation that balances landmark correspondence and smoothness. In recent years, conformal and quasi-conformal mappings have been considered for the analysis of medical and biological shapes such as brain cortical surfaces [12], hippocampi [13,14], vestibular systems [15], carotid arteries [16] and insect wings [17,18]. In particular, Teichmüller map, a special type of quasi-conformal maps, is advantageous in the sense that it allows for exact landmark matching and is associated with a constant conformal distortion, as well as a natural metric called the Teichmüller distance. The Teichmüller distances between shapes, together with the differences in curvature of the shapes, serve as a powerful tool for capturing and quantifying shape variation.

In anthropology, bioarchaeology and forensic science, a major problem is to obtain useful information from human remains. While it is possible to extract the DNA from the remains, the genetic information may be degraded during excavation or decomposition [19]. Also, the extraction process may create irreversible damages to the samples [20]. To avoid the above-mentioned issues, one possible alternative approach is to analyze the shape of the remains. Unlike tissues and skins, which decay significantly over time, teeth are morphologically stable and resistant to degradation. Hence, the shape analysis of teeth is important for interpreting information of gender, ancestry and other identifiable factors.

* Corresponding author.
E-mail address: lmlui@math.cuhk.edu.hk (L.M. Lui).

https://doi.org/10.1016/j.patcog.2019.107064
0031-3203/

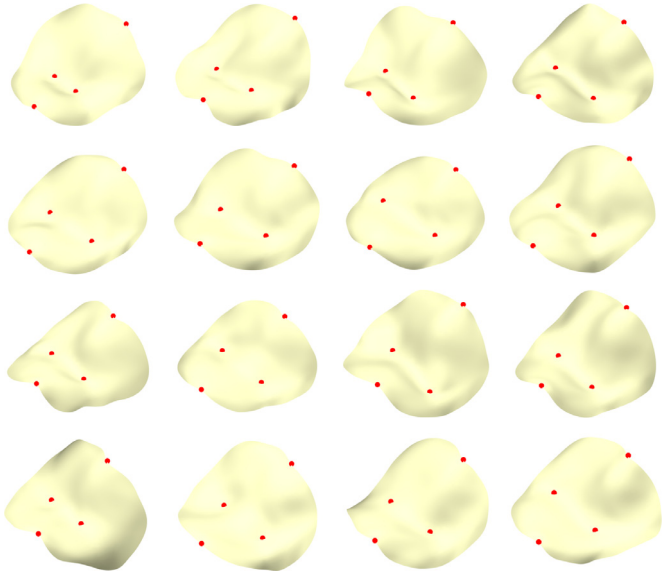

Fig. 1. Examples of the second upper premolar occlusal surfaces from two populations in Australia [26,27], with four landmarks of the buccal cusp, the lingual cusp, the mesial fossa pit and the distal fossa pit highlighted in red. Each row shows four specimens with the same ancestry and gender. First row: Indigenous males. Second row: Indigenous females. Third row: European males. Fourth row: European females. It can be observed that the surfaces are different in terms of the overall shape, curvature and landmark positions. (For interpretation of the references to colour in this figure legend, the reader is referred to the web version of this article.)

Traditional morphometric methods have been extensively used for the study of the human tooth variation in terms of tooth size [21], tooth weight [22] etc. To have a better understanding of the tooth shape variation, landmark-based geometric morphometric methods such as the Procrustes superimposition [10] and thin plate spline transformation [11] have been applied for studying the dental variation of different populations [23–25]. However, a well-known limitation of these mapping methods is that in general neither the entire tooth shapes nor the landmarks can be exactly matched. This inaccuracy may compromise the comparison between the geometry of different tooth shapes.

In this work, we propose a framework for accurately classifying a large set of 3D simply-connected open surfaces, by characterizing the shape variations using landmark-matching Teichmüller maps. The key to the unparalleled accuracy lies in taking into account the additional surface shape information using ideas from computational geometry and quasi-conformal theory. Illustration of our framework is done by applying the new algorithms to a dataset of tooth occlusal surfaces from Indigenous Australians [26] and Australians of European ancestry [27] (see Fig. 1 for examples). More specifically, to capture and quantify the shape differences between the 3D surfaces in terms of the overall shape, the curvature and the positions of the anatomical landmarks, we extend our previous work on landmark-matching Teichmüller map [28] to achieve an accurate 1-1 mapping between them, and further develop a quasi-conformal shape analysis model based on our previous work [14] for performing a classification. The classification results for the tooth dataset shed light on the ancestral variation and sexual dimorphism of teeth.

2. Mathematical background

We first review some important concepts in quasi-conformal theory. Readers are referred to [28–30] for more details.

2.1. Quasi-conformal map

Intuitively, quasi-conformal maps are orientation-preserving homeomorphisms with bounded conformality distortions. Under a quasi-conformal map, an infinitesimal circle is mapped to an infinitesimal ellipse with bounded eccentricity. The formal definition of quasi-conformal maps on the complex plane is given below.

Definition 2.1 (Quasi-conformal maps)**.** A quasi-conformal map $f: \mathbb{C} \to \mathbb{C}$ is a map satisfying the Beltrami equation $\frac{\partial f}{\partial \bar{z}} = \mu_f(z)\frac{\partial f}{\partial z}$, for some complex-valued function $\mu_f(z)$ with $\|\mu_f\|_\infty < 1$.

One can easily see that if $\mu_f = 0$, the above equation becomes the Cauchy-Riemann equation and hence f is conformal (i.e. angle preserving).

More generally, let S_1, S_2 be two Riemann surfaces in $\mathbb{R}^3$. A Beltrami differential $\mu(z)\frac{d\bar{z}}{dz}$ on a Riemann surface S is an assignment to each chart (U_α, ϕ_α) on an L_∞ complex-valued function μ_α, defined on local parameter z_α such that $\mu_\alpha \frac{\overline{dz_\alpha}}{dz_\alpha} = \mu_\beta \frac{\overline{dz_\beta}}{dz_\beta}$ on the domain which is also covered by another chart (U_β, ϕ_β). An orientation-preserving diffeomorphism $f: S_1 \to S_2$ is said to be a quasi-conformal map associated with the Beltrami differential $\mu(z)\frac{d\bar{z}}{dz}$ if for any chart (U_α, ϕ_α) on S_1 and any chart (U_β, ψ_β) on S_2, the map $f_{\alpha\beta} = \psi_\beta \circ f \circ \phi_\alpha^{-1}$ is a quasi-conformal map.

In case the surfaces are simply-connected open surfaces, they can be represented by a single chart. Then, the computation of quasi-conformal maps between them can be easily reduced to the computation on the complex plane via a composition of mappings. Below is a useful property concerning the Beltrami coefficient associated with a composition of quasi-conformal maps, also known as the composition formula.

Proposition 2.2 (Composition of quasi-conformal maps)**.** *If $f: \mathbb{C} \to \mathbb{C}$ and $g: \mathbb{C} \to \mathbb{C}$ are quasi-conformal maps, then $g \circ f$ is also a quasi-conformal map with Beltrami coefficient*

$$\mu_{g\circ f}(z) = \frac{\mu_f(z) + \frac{\overline{f_z}}{f_z}\mu_g(f(z))}{1 + \frac{\overline{f_z}}{f_z}\overline{\mu_f(z)}\mu_g(f(z))}. \tag{1}$$

From the above composition formula, it is easy to see that if f is conformal and g is quasi-conformal, then $\mu_{g\circ f}(z) = \mu_g(f(z))$ as $\mu_f = 0$. Also, if f is quasi-conformal and g is conformal, then $\mu_{g\circ f}(z) = \mu_f(z)$ as $\mu_g = 0$. In other words, the composition with a conformal map does not change the Beltrami coefficient.

2.2. Teichmüller map

Teichmüller map is a quasi-conformal map whose Beltrami coefficient has a constant norm. Hence, a Teichmüller map has a uniform conformal distortion over the entire domain. The formal definition of Teichmüller map is described below.

Definition 2.3 (Teichmüller map)**.** Let $f: S_1 \to S_2$ be a quasi-conformal map. f is said to be a *Teichmüller map (T-map)* associated with the quadratic differential $q = \varphi dz^2$ where $\varphi: S_1 \to \mathbb{C}$ is a holomorphic function if its associated Beltrami coefficient is of the form

$$\mu(f) = k\frac{\overline{\varphi}}{|\varphi|}, \tag{2}$$

for some constant $k < 1$ and quadratic differential $q \neq 0$ with $||q||_1 = \int_{S_1} |\varphi| < \infty$.

Furthermore, Teichmüller maps are closely related to a class of maps called extremal quasi-conformal maps.

Definition 2.4 (Extremal quasi-conformal map)**.** Let $f: S_1 \to S_2$ be a quasi-conformal map. f is said to be an extremal quasi-conformal

map if for any quasi-conformal map h: $S_1 \to S_2$ isotopic to f relative to the boundary, we have

$$K(f) \leq K(h), \tag{3}$$

where $K(f)$ is the maximal quasi-conformal dilation of f. It is uniquely extremal if the inequality (3) is strict when $h \neq f$.

The two above-mentioned concepts are connected by the following theorem.

Theorem 2.5 (Landmark-matching Teichmüller map [31])**.** *Let $g: \partial\mathbb{D} \to \partial\mathbb{D}$ be an orientation-preserving diffeomorphism of $\partial\mathbb{D}$, where $\mathbb{D}$ is the unit disk. Suppose further that $g'(e^{i\theta}) \neq 0$ and $g''(e^{i\theta})$ is bounded. Let $\{l^k\}_{k=1}^n \in \mathbb{D}$ and $\{q^k\}_{k=1}^n \in \mathbb{D}$ be the corresponding interior landmark constraints. Then there exists a unique Teichmüller map $f: (\mathbb{D}, \{l^k\}_{k=1}^n) \to (\mathbb{D}, \{q^k\}_{k=1}^n)$ matching the interior landmarks, which is the unique extremal extension of g to $\mathbb{D}$. Here $(\mathbb{D}, \{l^k\}_{k=1}^n)$ denotes the unit disk $\mathbb{D}$ with prescribed landmark points $\{l^k\}_{k=1}^n$.*

Therefore, besides equipped with uniform conformal distortion, Teichmüller maps are extremal in the sense that they minimize the maximal quasi-conformal dilation. Furthermore, Teichmüller maps induce a natural metric, called the *Teichmüller distance* [30], which can be used to measure the difference between two shapes in terms of local geometric distortion.

Definition 2.6 (Teichmüller distance)**.** For every i, let S_i be a Riemann surface with landmarks $\{p_i^k\}_{k=1}^n$. The *Teichmüller distance* between (f_i, S_i) and (f_j, S_j) is defined as

$$d_T((f_i, S_i), (f_j, S_j)) = \inf_{\varphi} \frac{1}{2} \log K(\varphi), \tag{4}$$

where $\varphi: S_i \to S_j$ varies over all quasi-conformal maps with $\{p_i^k\}_{k=1}^n$ corresponds to $\{p_j^k\}_{k=1}^n$, which is homotopic to $f_j^{-1} \circ f_i$, and K is the maximal quasi-conformal dilation.

3. Proposed method

In this section, we describe our proposed method for accurately classifying a large set of 3D simply-connected open surfaces. To characterize the shape variation in terms of the surface geometry as well as the prescribed landmarks on them, we first propose a method for computing landmark-matching Teichmüller maps between 3D surfaces. Then, with the Teichmüller mapping results, we further propose a shape classification model based on quasi-conformal theory.

3.1. Landmark-matching Teichmüller map between simply-connected open surfaces

Denote two simply-connected open surfaces by S_i and S_j, each with n landmarks $\{l_i^1, \ldots, l_i^n\}$ and $\{l_j^1, \ldots, l_j^n\}$. We aim to quantify the difference between the two surfaces using a landmark-matching Teichmüller map $f_{ij}: S_i \to S_j$ that satisfies $f_{ij}(l_i^k) = l_j^k$, $k = 1, \ldots, n$. Unlike other methods such as radial basis function and spline-based methods, our approach takes both the overall shape and the landmarks of the surfaces into account, and is guaranteed by quasi-conformal theory.

The procedure for finding f_{ij} is outlined in Fig. 2. It consists of three steps, namely the rectangular conformal parameterizations, the landmark-matching Teichmüller map between the rectangles and the composition. Below, we discuss the technical detail of each step.

3.1.1. Rectangular conformal parameterizations

To simplify the mapping problem, we begin with flattening S_i and S_j onto the plane. While there exists other flattening methods such as area-preserving maps [32,33], conformal parameterizations are preferred in our case as they preserve the Beltrami coefficient and hence the conformal distortion under compositions. Following the approach in [28], we compute two conformal maps $g_i: S_i \to R_i$ and $g_j: S_j \to R_j$ that flatten S_i and S_j onto two rectangular domains R_i, R_j on the plane.

Note that the rectangular conformal parameterization algorithm in [28] was developed for point clouds. In our case of surface morphometry here, the approximation of the differential operators in [28] can be replaced by the mesh-based approximations, which are much simpler and more accurate. The rectangular conformal parameterization algorithm in [28] consists of a step of conformally parameterizing a surface onto the unit disk and a step of conformally mapping the unit disk to a rectangle. Here, the disk conformal parameterization step can be replaced by our more recent disk conformal map algorithms [34,35] for accelerating the computation and improving the accuracy.

3.1.2. Landmark-matching Teichmüller map between the rectangular domains

We then proceed to compute the landmark-matching Teichmüller map $h_{ij}: R_i \to R_j$ between the rectangular domains, following the approach in [28]. In particular, to satisfy the landmark correspondences, we require that

$$h_{ij}(g_i(l_i^k)) = g_j(q_i^k), k = 1, \ldots, n. \tag{5}$$

Again, note that [28] was developed for point clouds while the mesh structure is available in our case here. Therefore, the numerical algorithm used in [28] can be replaced by the more efficient mesh-based QC Iteration algorithm [29].

Besides the landmark-matching Teichmüller map h_{ij}, we can also obtain the associated Beltrami coefficient $\mu_{h_{ij}}$. Since h_{ij} is Teichmüller, $\mu_{h_{ij}}$ is with uniform norm, i.e. $|\mu_{h_{ij}}|$ is a constant over the entire domain.

3.1.3. Composition for obtaining the landmark-matching Teichmüller map between the surfaces

With the rectangular conformal maps g_i, g_j and the landmark-matching Teichmüller map h_{ij}, a map $f_{ij}: S_i \to S_j$ can be obtained by $f_{ij} = g_j^{-1} \circ h_{ij} \circ g_i$. Note that for any landmark l_i^k, we have

$$f_{ij}(l_i^k) = g_j^{-1} \circ h_{ij} \circ g_i(l_i^k) = g_j^{-1}(h_{ij}(g_i(l_i^k))) = g_j^{-1}(g_j(q_i^k)) = q_i^k. \tag{6}$$

Hence, f_{ij} is a landmark-matching map between S_i and S_j.

Furthermore, the conformal distortion of f_{ij} is the same as the conformal distortion of h_{ij}. In other words, f_{ij} achieves a uniform conformal distortion $|\mu_{h_{ij}}|$ and hence f_{ij} is a Teichmüller map. This can be explained by the composition formula (1). Since g_i, g_j are conformal, we have $\mu_{g_i} = \mu_{g_j} = 0$. Now, by the composition formula, we have

$$\begin{aligned} \mu_{h_{ij} \circ g_i}(z) &= \frac{\mu_{g_i}(z) + \frac{\overline{g_{iz}}}{g_{iz}} \mu_{h_{ij}}(g_i(z))}{1 + \frac{\overline{g_{iz}}}{g_{iz}} \overline{\mu_{g_i}(z)} \mu_{h_{ij}}(g_i(z))} = \frac{0 + \frac{\overline{g_{iz}}}{g_{iz}} \mu_{h_{ij}}(g_i(z))}{1 + 0} \\ &= \frac{\overline{g_{iz}}}{g_{iz}} \mu_{h_{ij}}(g_i(z)), \end{aligned} \tag{7}$$

which implies that

$$|\mu_{h_{ij} \circ g_i}(z)| = \left| \frac{\overline{g_{iz}}}{g_{iz}} \mu_{h_{ij}}(g_i(z)) \right| = |\mu_{h_{ij}}(g_i(z))| = |\mu_{h_{ij}}|. \tag{8}$$

Similarly,

$$|\mu_{f_{ij}}(z)| = |\mu_{g_j^{-1}\circ h_{ij}\circ g_i}(z)| = |\mu_{h_{ij}\circ g_i}(z)| = |\mu_{h_{ij}}(g_i(z))| = |\mu_{h_{ij}}|. \tag{9}$$

As a consequence, the Teichmüller distance is also uniquely determined by the maximal quasi-conformal dilation of the extremal map between the two rectangular domains. The Teichmüller distance d between the two surfaces S_i and S_j is then given by $d_{ij} = \frac{1}{2}\log\frac{1+|\mu_{h_{ij}}|}{1-|\mu_{h_{ij}}|}$.

This completes the computation of the landmark-matching Teichmüller map between the two surfaces. The algorithm is summarized in Algorithm 1 (see Fig. 2 for a graphical illustration).

Algorithm 1: Landmark-matching Teichmüller map between simply-connected open surfaces.

Input: Two simply-connected open surfaces S_i, S_j with landmarks $\{l_i^1, \dots, l_i^n\}$ and $\{l_j^1, \dots, l_j^n\}$.

Output: A landmark-matching Teichmüller map $f_{ij} : S_i \to S_j$, the Teichmüller distance d_{ij}.

1 Compute disk conformal parameterizations of S_i and S_j using the linear disk conformal map algorithm [35];
2 Using the linear disk conformal map algorithm [35] and the disk-to-rectangle conformal map algorithm [28], obtain rectangular conformal parameterizations $g_i : S_i \to \mathbb{R}^2$ and $g_j : S_j \to \mathbb{R}^2$;
3 Using the QC Iteration algorithm [29], compute the landmark-matching Teichmüller map $h_{ij} : g_i(S_i) \to g_j(S_j)$ and obtain the Beltrami coefficient $\mu_{h_{ij}}$;
4 Obtain $f_{ij} = g_j^{-1} \circ h_{ij} \circ g_i$ and $d_{ij} = \frac{1}{2}\log\frac{1+|\mu_{h_{ij}}|}{1-|\mu_{h_{ij}}|}$;

3.2. Quasi-conformal statistical shape analysis

Note that the landmark-matching Teichmüller maps do not only provide us with a quantitative measure of the local geometric distortion of surfaces but also an accurate 1-1 correspondence between different parts of them. As illustrated in Fig. 3, the mean and Gaussian curvatures also effectively quantify the surface geometry. With the aid of the landmark-matching Teichmüller maps, it is possible for us to analyze the surface shapes in terms of both the local geometric distortion and the curvature differences. Below, we devise a quasi-conformal statistical shape analysis model for building a surface classification machine.

Suppose we are given a database of simply-connected open surfaces $\{S_i\}_{i=1}^N$, with m of them being labelled as class "A" and n of them being labelled as class "B" (i.e. $m+n=N$). We first compute the landmark-matching Teichmüller maps f_i: $S_i \to S$ from every S_i to their mean surface S. We can then obtain the associated Teichmüller distance d_i. Also, for each S_i, we compute the mean curvature H_i and the Gaussian curvature K_i at every vertex of it. After obtaining the results for all surfaces, a classification model can be built based on d_i, H_i, and K_i. More specifically, given a landmark-matching Teichmüller map f_i: $S_i \to S$, the following shape index E_{shape} is considered:

$$E_{\text{shape}}(f_i)(v^k) = \alpha|H_i(v^k) - H(f_i(v^k))| + \beta|K_i(v^k) - K(f_i(v^k))| + \gamma d_i. \tag{10}$$

Here H, K represent the mean and Gaussian curvature of the mean surface S, v^k are the vertices of S_i with $k = 1, 2, \dots, M$, and α, β, γ are real nonnegative scalar parameters. Without loss of generality, we assume $\alpha^2+\beta^2+\gamma^2 = 1$. Note that E_{shape} is a complete shape index for measuring all kind of distortion of the mapping f_i. The first two terms measure the curvature deviation of the mapping, and the third term measures the local geometric distortion of the mapping. In particular, $E_{\text{shape}} \equiv 0$ if and only if the two surfaces are identical up to rigid motion.

When compared to the formulation of shape index in [14], the shape index E_{shape} here consists of the same first two terms while the third term is different. More specifically, here we use the Teichmüller distance d_i instead of the norm of the Beltrami coefficient $|\mu_i(v^k)|$ for the third term. Note that by quasi-conformal theory, $|\mu_i(v^k)|$ is always bounded by [0, 1] for any bijective mappings. Instead, the Teichmüller distance is a metric and lies within $[0, \infty)$. As the first two terms $|H_i(v^k) - H(f_i(v^k))|$ and $|K_i(v^k) - K(f_i(v^k))|$ also have range $[0, \infty)$, using the Teichmüller distance as the third term gives a better balance between the three terms. Also, since f_i is a Teichmüller map, d_i is constant over the entire domain. Instead of the vertex-wise evaluation of $|\mu_i(v^k)|$, we can use a single scalar d_i to capture the quasi-conformal distortion between S_i and S.

Using the shape index function E_{shape}, a feature vector $\mathbf{c}_i = (c_i^1, c_i^2, \dots, c_i^M)$ can be computed for each surface, with $c_i^k = E_{\text{shape}}(f_i)(v^k)$. Combining all feature vectors, we obtain a feature matrix $C = (\mathbf{c_1}, \mathbf{c_2}, \cdots, \mathbf{c_N})$. The feature matrix provides full information of all shapes at every vertex on the surface. However, it is not necessarily true that all parts of the surfaces (i.e. all rows in C) are statistically significant for the desired classification. To extract the statistically significant regions that are the most related to the classification from the surfaces, the bagging predictors [36] are applied to extract only those vertices having a p-value less than or equal to a non-negative threshold parameter $p_{cut} \in [0, 1]$. Therefore, we obtained the truncated feature matrix $\hat{C} = (\hat{\mathbf{c}}_1, \hat{\mathbf{c}}_2, \cdots, \hat{\mathbf{c}}_N)$, where $\hat{\mathbf{c}}_i = (c_i^{j_1}, \dots, c_i^{j_m})$. Afterwards, the mean feature vector $\mathbf{c}_{mean}$ is computed over all the m feature vectors associated to those surfaces labelled as class "A". The distance $d_i = ||\hat{\mathbf{c}}_i - \mathbf{c}_{mean}||_2$ of each feature vector to the mean feature vector is computed. Since $\mathbf{c}_{mean}$ is the mean of the feature vectors of class "A", d_i should be small if the surface S_i is labelled as class "A" and d_i should be large if the surface S_i is labelled as class "B". Under this assumption, we can compute the best cutting parameter $\delta > 0$ maximizing the probability that $d_i < \delta$ for all surfaces S_i from class "A" and $d_i > \delta$ for all surfaces S_i from class "B". This gives a classification model, that whenever a new surface S_{new} is given, by computing the corresponding $\hat{\mathbf{c}}_{new}$ and hence d_{new} following the above pipelines, S_{new} can be automatically classified as group "A" if $d_{new} < \delta$, or as group "B" if $d_{new} > \delta$. Readers are referred to [14] for more details of the classification model.

Now, given a set of shapes and a binary classification criterion (e.g. classifying all tooth shapes into two ancestral/gender groups), we determine the optimal shape index parameters (α, β, γ) and the optimal threshold parameter p_{cut} that yield the highest classification accuracy. To search for the optimal (α, β, γ), the following *spherical marching scheme* (SMS) is utilized. Since we assume that $\alpha^2+\beta^2+\gamma^2 = 1$, the space of the shape index parameters $\{(\alpha, \beta, \gamma) \in \mathbb{R}^3 : \alpha^2+\beta^2+\gamma^2 = 1\}$ can be regarded as the unit sphere $\mathbb{S}^2$. Then, in order to search for the best set of parameters (α, β, γ) over $\mathbb{S}^2$ to maximize the classification accuracy in a timely manner, we parameterize $\mathbb{S}^2$ using the spherical coordinates

$$\mathbb{S}^2 = \{(\sin(\theta)\cos(\varphi), \sin(\theta)\sin(\varphi), \cos(\theta)) \in \mathbb{R}^2 : \theta \in [0, \pi], \varphi \in [0, 2\pi)\}. \tag{11}$$

Now, we discretize the parameter domain $[0,\ \pi] \times [0,\ 2\pi)$ using regular gridding with density $\rho > 0$, i.e.

$$[0, \pi] \times [0, 2\pi) \approx \Omega = \left\{ (n\rho, m\rho) \in \mathbb{R}^2 : n = 0, 1, \ldots, \frac{\pi}{\rho}, m = 0, 1, \ldots, \frac{2\pi}{\rho} \right\}. \quad (12)$$

Then, for each n, m, $(n\rho, m\rho)$ corresponds to a set of parameters

$$(\alpha, \beta, \gamma)_{n,m} = (\sin(n\rho)\cos(m\rho), \sin(n\rho)\sin(m\rho), \cos(n\rho)) \quad (13)$$

on $\mathbb{S}^2$, and hence we can compute the classification accuracy of the proposed model using this set of parameters $(\alpha,\ \beta,\ \gamma)_{n,m}$. Therefore, the optimal $(\alpha,\ \beta,\ \gamma)$ can be chosen as the set of $(\alpha,\ \beta,\ \gamma)_{n,m}$ that gives the highest classification accuracy among all n, m. In practice, the density parameter ρ is chosen within $[0.01\pi,\ 0.03\pi]$. The optimal threshold parameter p_{cut} for the extraction of statistically significant regions is determined by testing among different magnitudes of 10^k, with $k = 0, -1, -2, -3, -4$. The quasi-conformal shape classification algorithm is summarized in Algorithm 2 (see also Fig. 4).

Algorithm 2: Quasi-conformal shape classification.

Input: A set of simply-connected open surfaces $\{S_i\}_{i=1}^N$ with prescribed landmarks, and a classification criterion.

Output: The classification result and the optimal parameters $\alpha, \beta, \gamma, p_{cut}$.

1 Compute the mean surface S of $\{S_i\}_{i=1}^N$;
2 Compute the landmark-matching Teichmüller map $f_i : S_i \to S$ and the Teichmüller distance d_i for all i;
3 For all i and for all k, evaluate the mean curvature difference $|H_i(v^k) - H(f_i(v^k))|$ and the Gaussian curvature difference $|K_i(v^k) - K(f_i(v^k))|$;
4 Search for the optimal parameters $\alpha, \beta, \gamma, p_{cut}$ such that the shape index E_{shape} and the statistically significant vertices together give the best classification result;

It is noteworthy that the optimal shape index parameters $(\alpha,\ \beta,\ \gamma)$ determined by our model do not only maximize the classification accuracy with respect to a given criterion but also help us analyze the shape difference between the surfaces. More specifically, note that the mean and Gaussian curvatures uniquely determine a surface up to rigid motions, while the Teichmüller distance encodes the local geometric distortion. By changing the shape index parameters $(\alpha,\ \beta,\ \gamma)$ and comparing the corresponding classification accuracies, we can study the importance of each component (the mean curvature difference, the Gaussian curvature difference and the Teichmüller distance) for the classification and determine the major factor that distinguishes the surfaces.

The MATLAB codes of the two proposed algorithms are available at [37].

4. Data description

4.1. Study subjects

Our study focuses on 140 subjects from two populations in Australia, namely the Indigenous group (subjects of Indigenous Australian ancestry) and the European group (subjects of European ancestry). The Indigenous group consists of 70 subjects (35 females, 35 males) of the Walpiri people (a group of Indigenous Australians who speak the Warlpiri language) living at Yuendumu in the Northern Territory of Australia [26]. The European group consists of 70 subjects (35 females, 35 males) with parents of Southern or Western European origin obtained from the Australian Twin study [27], with one co-twin from each twin pair selected randomly. The dental casts of the permanent dentitions of the subjects were obtained from the Yuendumu and Australian Twin collections housed in the Murray James Barrett Laboratory, Adelaide Dental School, The University of Adelaide. To overcome the problem of advanced tooth wear rate for Indigenous Australians due to hunter-gatherer dietary practices [38] in the Yuendumu collection, assessment was limited to subjects in their early teens, with recently erupted premolars. Mean ages of the subjects were 12 years and 5 months (Indigenous females), 13 years (Indigenous males), 14 years and 8 months (European females), and 15 years and 7 months (European males). Readers are referred to [25] for a more detailed description of the dataset.

4.2. Data acquisition and pre-processing

The detailed procedure for the tooth data acquisition and the landmark protocol were described in [25]. The dental casts of the subjects were scanned using a 3D scanner at the resolution of 80-μm point distance. The segmented.stl files were imported in Viewbox 4 software (dHAL software, Kifissia, Greece) for digitization. The upper second premolar in the maxillary right quadrant of each subject was extracted for this study.

Fixed landmarks were assigned based on established protocols in hominin premolars [39,40] and curve and surface semi-landmarks followed the procedures by Polychronis et al. [24]. Detailed steps of the landmarking protocol are provided in [25], but essential steps are highlighted in here. The first major step is to create a template before applying the established landmark template on remaining specimens. An upper second premolar tooth was randomly selected and four fixed landmarks were placed on it (two on the buccal and lingual cusp tips, and two in the pits of the mesial and distal fossae). Fixed landmarks provide stable and repeatable landmarks as they are easily definable in each specimen. Following this, eighteen semi-landmarks were placed along the major ridges of each tooth to delineate the occlusal circumference. A curve was drawn over the mesial and distal ridges respectively, connecting the buccal and lingual cusp tips. Nine equidistant semi-landmarks were placed on each curve. Finally, surface semi-landmarks were added to the occlusal surface by using the highlighting tool on Viewbox 4, so that they are not superimposed on placed fixed landmarks and curve semi-landmarks. The landmark template was applied to the remaining specimens. Fixed landmarks and curve semi-landmarks were placed manually on each specimen. Subsequently, surface semi-landmarks were transposed using thin plate spline transformation [11]. The curved and surface semi-landmarks were allowed to slide to minimize bending energy between each premolar configuration and the reference specimen. Following this, re-projection of semi-landmarks on respective curves and surfaces was repeated six times to ensure convergence. This resulted in 4 landmarks and 88 curve and surface semi-landmarks for each tooth.

For our surface-based morphometric approach, it is desirable to represent the occlusal surfaces using triangle meshes. To achieve the triangle mesh representation, we first triangulated the landmarks and semi-landmarks of the occlusal surfaces. We then enhanced the mesh quality and resolution by surface remeshing [41], thereby obtaining smooth, high-quality triangle meshes for our subsequent surface morphometry. Each remeshed occlusal surface consists of 1217 vertices.

For each remeshed occlusal surface S_i, denote the four landmarks of the buccal cusp, lingual cusp, mesial fossa pit and distal fossa pit by $l_i^1, l_i^2, l_i^3, l_i^4$ respectively. Note that above-mentioned rectangular conformal parameterization procedure involves specifying four vertices on each occlusal surface to be mapped to the four corners of the corresponding rectangular domain. It is

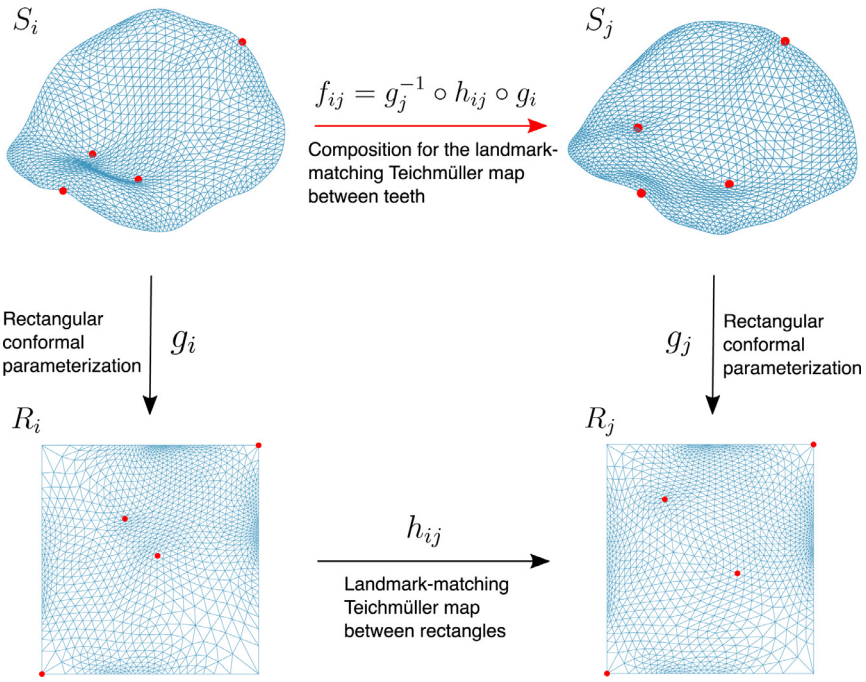

Fig. 2. An illustration of the computation of the landmark-matching Teichmüller map f_{ij} between two occlusal surfaces S_i and S_j (landmarks highlighted in red). The two surfaces are first flattened onto the plane by two rectangular conformal parameterizations g_i and g_j. The landmark-matching Teichmüller map h_{ij} between the two rectangles is then computed. Finally, the landmark-matching Teichmüller map f_{ij} between the surfaces is given by the composition $g_j^{-1} \circ h_{ij} \circ g_i$. (For interpretation of the references to colour in this figure legend, the reader is referred to the web version of this article.)

natural to consider the two crest landmarks l_i^1, l_i^2 on the boundary of the tooth surface as two corners, and the two other points on the boundary closest to the pit landmarks l_i^3, l_i^4 as the other two corners (see the bottom part of Fig. 2 for an illustration). This ensures an accurate correspondence between the rectangular domains for different tooth surfaces.

5. Results

5.1. Landmark-matching Teichmüller map of occlusal surfaces

As for a demonstration of our proposed method, we compute the landmark-matching Teichmüller map f_{ij} between the occlusal surfaces S_i and S_j shown in Fig. 2. We remark that S_i is an Indigenous male sample and S_j is an European female sample. Fig. 5 shows the mapping result and the curvature differences between the two surfaces. Comparing the mapping result in Fig. 5 and the original surfaces shown in Fig. 2, it can be observed that S_i is completely mapped onto S_j under the mapping f_{ij}, with the landmarks exactly matched. The histogram of the norm of the Beltrami coefficients $|\mu_{f_{ij}}|$ is highly concentrated at one value, indicating that the mapping is Teichmüller. Also, using the landmark-matching Teichmüller map, we can easily evaluate the mean and Gaussian curvature differences between the two surfaces, thereby quantifying the shape difference between them. It is noteworthy that the major difference in Gaussian curvature is located at the fossa pits, while the difference in mean curvature is relatively widespread over the surfaces.

5.2. Classification of the 140 upper second premolars with respect to ancestry and gender

After demonstrating the effectiveness of the landmark-matching Teichmüller map for quantifying tooth shape difference, we deploy the mapping algorithm and the quasi-conformal statistical shape analysis model on the 140 upper second premolars in the dataset.

5.2.1. The classification accuracy

We first perform the classifications of all 140 occlusal surfaces in the dataset with respect to ancestry and gender using our proposed model. For comparison, we evaluate the classification accuracy achieved by our model as well as that achieved by two other classification methods respectively based on traditional morphometrics and landmark-based geometric morphometrics. More specifically, we consider the area-based classification [42,43] (note that the method in [42,43] was originally volume-based for genus-0 surfaces, and so its analogue for simply-connected open surfaces is area-based) and the Procrustes-based classification [25].

Table 1 summarizes the classification results obtained by the two previous methods and our proposed method. It can be observed that the area-based method results in low classification accuracy for both classification tasks, which suggests that the traditional morphometric methods are incapable of capturing the tooth shape variation. The Procrustes-based method gives a satisfactory result for the classification with respect to ancestry but not gender. This implies that while earlier methods in landmark-based geometric morphometrics are more capable than the traditional morphometric methods, they are still insufficient for detecting certain kinds of tooth shape variation. In contrast to the two previous methods, our proposed method achieves 98.57% accuracy (138 correct assignments out of 140 subjects) for the classification with respect to ancestry, and 97.14% accuracy (136 correct assignments out of 140 subjects) for the classification with respect to gender. In both tasks, our method outperforms the existing methods. In particular, for the classification with respect to gender, the accuracy of our method is higher than the existing methods by around 30%. This demonstrates the effectiveness of our proposed framework for tooth shape analysis.

5.2.2. The optimal parameters obtained by our model and their implications

To have a better understanding, we analyze the optimal parameters obtained by our model for the two classification tasks.

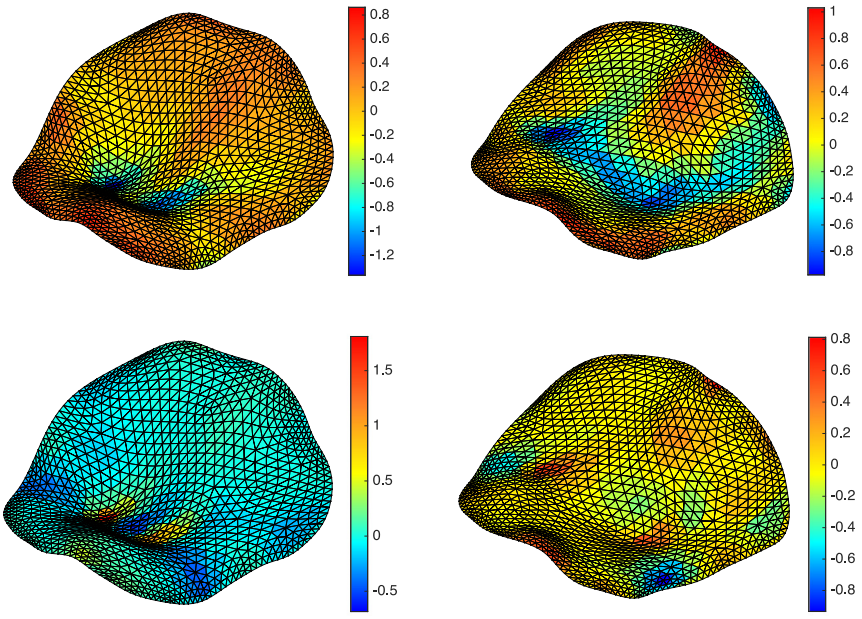

Fig. 3. Quantifying tooth geometry using mean and Gaussian curvatures. Top row: The mean curvature H of two occlusal surfaces. Bottom row: The Gaussian curvature K of them. An accurate comparison between the curvatures of different occlusal surfaces is made possible using landmark-matching Teichmüller maps.

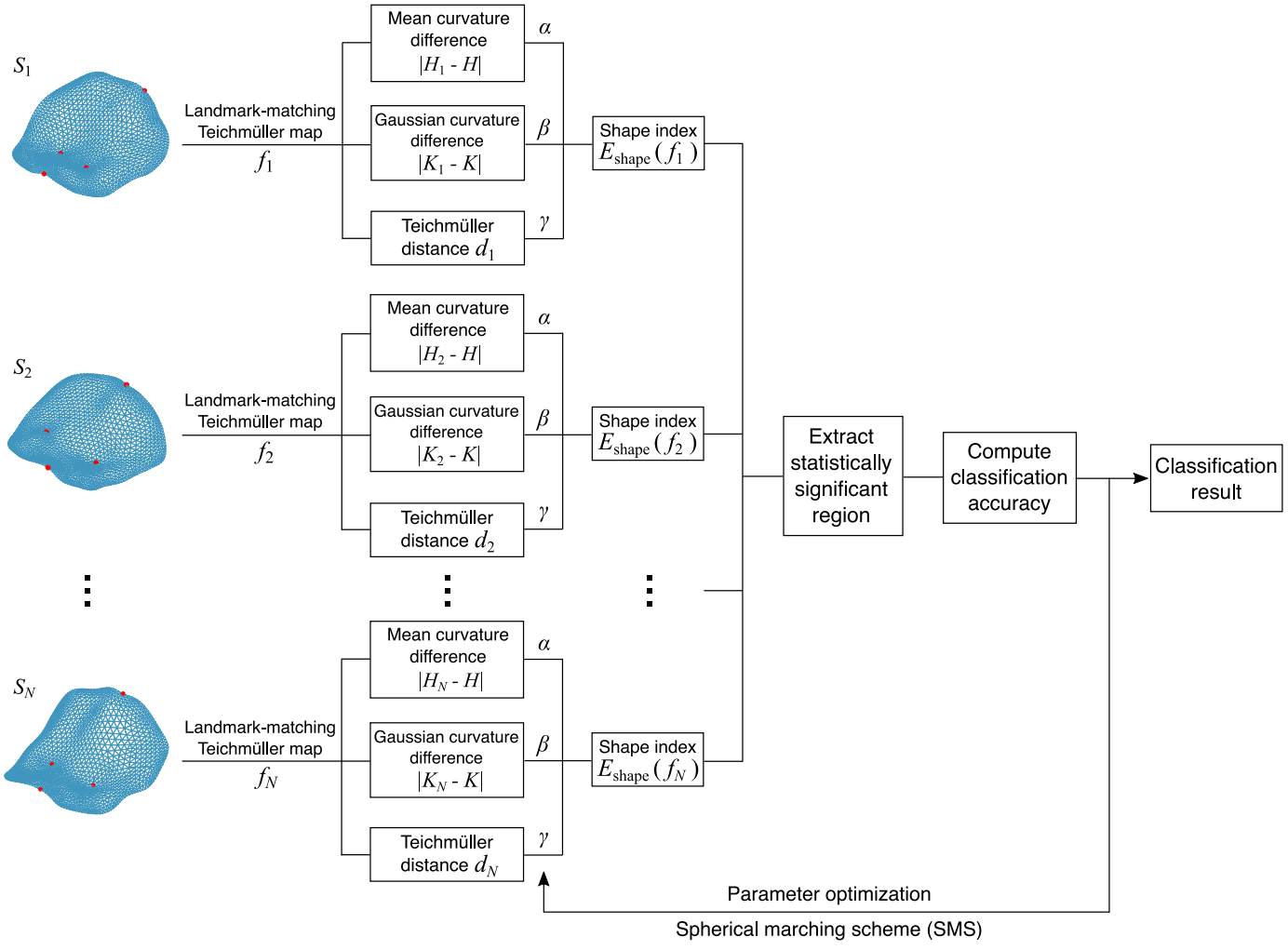

Fig. 4. An illustration of the quasi-conformal shape classification algorithm.

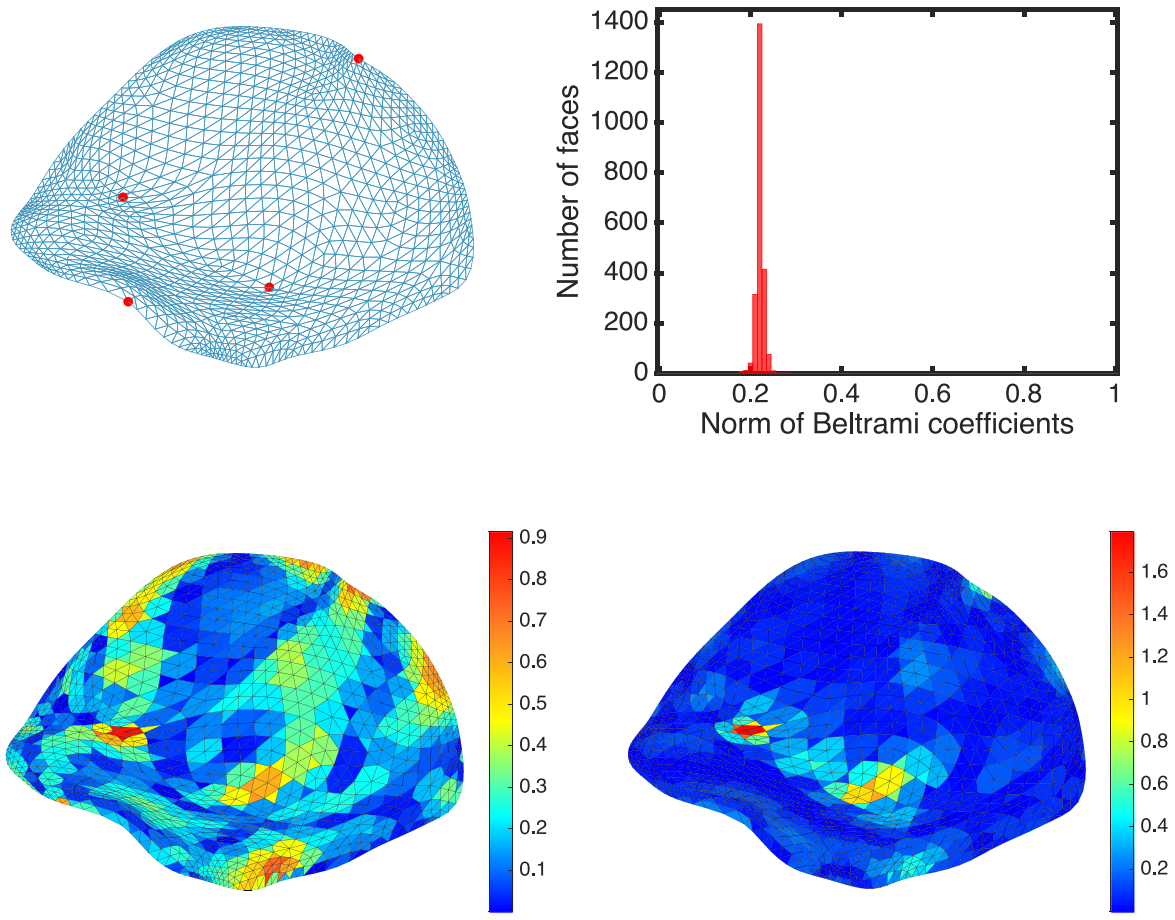

Fig. 5. The landmark-matching Teichmüller map between the two occlusal surfaces S_i, S_j shown in Fig. 2. Top left: The landmark-matching Teichmüller mapping result $f_{ij}(S_i)$. Top right: The histogram of $|\mu_{f_{ij}}|$. Bottom left: The mean curvature difference $|H_i(v) - H_j(f_{ij}(v))|$ between the two occlusal surfaces. Bottom right: The Gaussian curvature difference $|K_i(v) - K_j(f_{ij}(v))|$ between the two occlusal surfaces.

Table 1
Classification accuracy for all the 140 upper second premolars with respect to ancestry and gender obtained by the area-based method [42,43], the Procrustes-based method [25] and our method.

Classification Criterion	Overall Accuracy (Area-based [42,43])	Overall Accuracy (Procrustes-based [25])	Overall Accuracy (Our Method)
Ancestry	67.14%	91.43%	**98.57%**
Gender	51.43%	68.57%	**97.14%**

As shown in Table 2, the optimal parameters for achieving the maximum classification accuracy with respect to ancestry are $(\alpha, \beta, \gamma) = (0.1910, 0.2034, 0.9603)$, with $p_{cut} = 0.1$. From the values of α, β, γ, it can be observed that the Teichmüller distance plays the most significant role in the classification with respect to ancestry. To study whether all the three terms (mean curvature difference, Gaussian curvature difference, Teichmüller distance) in the shape index are necessary for yielding an accurate classification, we consider setting one of α, β, γ to be 0 and evaluating the accuracy. We observe that dropping any of these terms will lead to a significant decrease in the accuracy. This implies that while the optimal α and β are much smaller than γ, all the three terms are in fact important for the classification with respect to ancestry. In other words, the shape difference between the teeth from different ancestries is captured by the conformal (i.e. local geometric) distortion as well as the curvature differences.

Next, we consider varying the threshold parameter p_{cut} and obtaining the best parameters (α, β, γ) that maximize the classification accuracy for different p_{cut}. In general, a larger p_{cut} leads to a larger number of vertices identified as statistically significant by our model, and $p_{cut} = 1$ treats all vertices as statistically significant. Among several choices of p_{cut}, we observe that $p_{cut} = 0.1$ gives the highest classification accuracy. This suggests that using the entire surfaces does not necessarily lead to the best classification. Instead, it is important to extract certain regions on the surfaces which capture the shape difference between the Indigenous teeth and European teeth.

A similar analysis on the choices of the parameters can be performed for the classification with respect to gender (Table 3). The optimal parameters for achieving the maximum accuracy are $(\alpha, \beta, \gamma) = (0.2330, 0.0147, 0.9724)$, with $p_{cut} = 0.001$. This time, it can be observed that the Teichmüller distance term is dominant in the shape index, while the Gaussian curvature difference term is with an extremely small weight. By setting one of α, β, γ to be zero, we can see that dropping the mean curvature difference term or the Gaussian curvature difference term in the shape index

Table 2
Classification results for all the 140 upper second premolars with respect to ancestry for various choices of the shape index parameters α, β, γ and the threshold parameter p_{cut}. Here, $\#\nu$ is the number of statistically significant vertices extracted by our model under the parameter settings. The correct Indigenous rate is calculated by $\frac{\#\text{ of Indigenous subjects being classified as Indigenous}}{\text{Total \# of Indigenous subjects(i.e. 70)}}$, the correct European rate is calculated by $\frac{\#\text{ of European subjects being classified as European}}{\text{Total \# of European subjects (i.e. 70)}}$, and the overall accuracy is evaluated over all the 140 subjects.

Parameters					Classification Result w.r.t. Ancestry			
Description	α	β	γ	p_{cut}	$\#\nu$	Correct Indigenous Rate	Correct European Rate	Overall Accuracy
Optimal	**0.1910**	**0.2034**	**0.9603**	**0.1**	**288**	**0.9857**	**0.9857**	**0.9857**
No H term	0	0.2034	0.9603	0.1	129	0.0286	0.9286	0.4786
No K term	0.1910	0	0.9603		108	0.6857	0.4571	0.5714
No d term	0.1910	0.2034	0		535	0.5429	0.8143	0.6786
Varying	0.0922	0.9749	0.2028	0.0001	54	0.8286	0.8286	0.8286
p_{cut}	0.2761	0.6974	0.6613	0.001	79	0.8429	0.8000	0.8214
	0.1421	0.7449	0.6518	0.01	211	0.9714	0.9857	0.9786
	0.1910	**0.2034**	**0.9603**	**0.1**	**288**	**0.9857**	**0.9857**	**0.9857**
	0.6956	0.1786	0.6959	1	1217	0.6571	0.7143	0.6857

Table 3
Classification result for all the 140 upper second premolars with respect to gender for various choices of the shape index parameters α, β, γ and the threshold parameter p_{cut}. Refer to Table 2 for the description of the terms.

Parameters					Classification Result w.r.t. Gender			
Description	α	β	γ	p_{cut}	$\#\nu$	Correct Male Rate	Correct Female Rate	Overall Accuracy
Optimal	**0.2330**	**0.0147**	**0.9724**	**0.001**	**468**	**0.9857**	**0.9857**	**0.9857**
No H term	0	0.0147	0.9724	0.01	1217	0.9429	0.9857	0.9643
No K term	0.2330	0	0.9724		478	0.9857	0.9857	0.9857
No d term	0.2330	0.0147	0		0	N/A	N/A	N/A
Varying	0.187	0.0118	0.9823	0.0001	185	0.9857	0.9857	0.9857
p_{cut}	**0.2330**	**0.0147**	**0.9724**	**0.001**	**468**	**0.9857**	**0.9857**	**0.9857**
	0.0281	0.1093	0.9936	0.01	1188	0.9571	0.9857	0.9714
	0.0351	0.1841	0.9823	0.1	1198	0.9429	0.9857	0.9643
	0	0.9049	0.4258	1	1217	0.9714	0.9857	0.9786

do not affect the classification accuracy much. By contrast, dropping the Teichmüller distance term will even lead to zero statistically significant vertices and hence the classification cannot be done. In other words, the shape difference between teeth from different genders is mostly captured by the local geometric distortion but not the curvature differences. Again, by varying p_{cut} and evaluating the accuracy based on the corresponding optimal parameters, it can be observed that taking too many or too few vertices will lead to a sub-optimal result for the classification with respect to gender.

5.2.3. The statistically significant regions on the occlusal surfaces for the two classification tasks

We compare the statistically significant regions identified by our proposed model for the two classification criteria. As recorded in Tables 2 and 3, around 20% of the vertices (288 out of 1217 per surface) are statistically significant for the classification with respect to ancestry, while around 40% (468 out of 1217 per surface) are statistically significant for the classification with respect to gender. In other words, the classification with respect to gender requires more global information. We visualize the regions by highlighting the relevant vertices in the mean surface of all teeth (see Fig. 6). It can be observed that the statistically significant regions for the classification with respect to ancestry are primarily around the fossa pits, while those for the classification with respect to gender are primarily around the cusps.

5.2.4. Reliability of the model

Note that in the model, (α, β, γ) is optimized to maximize the classification accuracy. To check with the overfitting issue, we perform the following test. Recall that we have altogether 140 subjects in the dataset. With $(\alpha, \beta, \gamma) = (0.1910, 0.2034, 0.9603)$ being fixed, we perform 140 classification experiments with respect to ancestry. In the ith experiment, the ith subject is taken out from the dataset. A leave-one-out test is then performed on the remaining 139 subjects. Here we emphasize that the parameter setting is fixed to be $(\alpha, \beta, \gamma) = (0.1910, 0.2034, 0.9603)$, which may not be the optimal parameters for the dataset of the remaining 139 subjects. In this manner, altogether we have 140 leave-one-out tests under a constant parameter setting. Each test gives a classification accuracy, and the 95% confidence interval of these classification accuracies is $97.73\% - 98.84\%$. This suggests that our methodology does not lead to overfitting.

5.2.5. Possible explanation for the improvement achieved by our model when compared to the existing methods

It is natural to ask why our method is capable of achieving a significant improvement in classification accuracy when compared to the existing methods, especially for the classification with respect to gender. In fact, this can possibly be explained by the optimal parameters obtained by our model for the two classification tasks.

Note that the Procrustes-based method [25] aligns the teeth by rigid motions and studies their shape difference. Since the mean and Gaussian curvatures uniquely determine a surface up to rigid motions, the shape information captured by the Procrustes approach can be considered as that captured by the two curvature terms in our shape index. As we have analyzed above, the Teichmüller distance is the only significant factor in the shape index for the classification with respect to gender. Therefore, with the consideration of the Teichmüller distance in our proposed model, it is reasonable that we can achieve a significant improvement in the classification accuracy with respect to gender. As for the classification with respect to ancestry, we have pointed out above that both the curvature differences and the Teichmüller distance are important. Therefore, it is again reasonable that the Procrustes approach [25] achieves satisfactory accuracy, and our proposed model leads to an even better result.

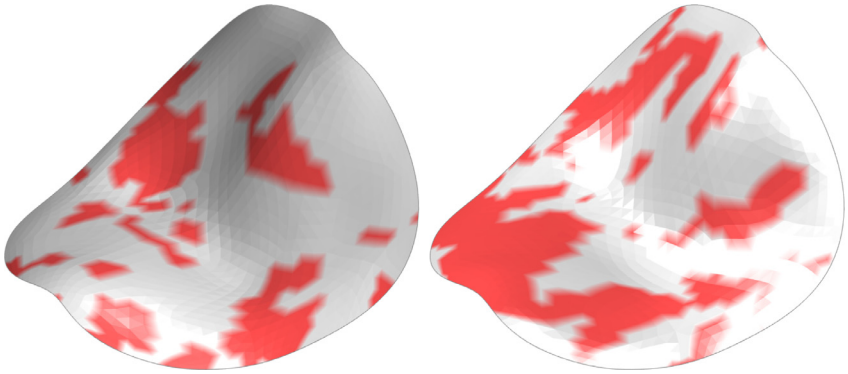

Fig. 6. The statistically significant regions (highlighted in red) extracted by our algorithm for the classifications with respect to ancestry (left) and gender (right), visualized on the mean surface of the 140 occlusal surfaces. (For interpretation of the references to colour in this figure legend, the reader is referred to the web version of this article.)

Table 4
The optimal parameters α, β, γ, p_{cut} and the accuracy of our proposed model for the classification with respect to ancestry within each gender group (each with size = 70).

Gender Group (size = 70)	α	β	γ	p_{cut}	Ancestry Classification Accuracy
Female	0.1950	0.0661	0.9786	0.01	0.9714
Male	0.0912	0.0234	0.9956	0.01	0.9714

Table 5
The optimal parameters α, β, γ, p_{cut} and the accuracy of our proposed model for the classification with respect to gender within each ancestral group (each with size = 70).

Ancestral Group (size = 70)	α	β	γ	p_{cut}	Gender Classification Accuracy
Indigenous	0.0940	0.0829	0.9921	0.01	0.9714
European	0.1702	0.1813	0.9686	0.01	0.9714

5.3. Classifications over subgroups

Besides performing the classifications over the entire set of 140 subjects, we consider the classifications over subgroups. More specifically, we study whether the classification with respect to ancestry within each gender group and the classification with respect to gender within each ancestral group are similar to the ones over the entire set of 140 subjects.

We first consider the classification with respect to ancestry within each gender group (female/male, each with 70 subjects in total). For each gender group, we compute a landmark-matching Teichmüller map for each surface and repeat the classification procedure on the 70 mapping results for classifying the teeth with respect to ancestry. As shown in Table 4, our method achieves over 97% classification accuracy for both gender groups. Also, in the two sets of optimal shape index parameters, γ is much greater than α and β. This suggests that our findings for the classification with respect to ancestry over the entire dataset also hold when we consider the classification among females and males separately. In other words, the aforementioned shape difference between the two ancestries can be found in both genders.

We then consider the classification with respect to gender within each ancestral group (Indigenous/European, each with 70 subjects in total). As shown in Table 5, our method achieves over 97% classification accuracy for both ancestral groups. Similarly to the above findings, the result suggests that the aforementioned shape difference between the two genders can be found in both ancestries.

6. Conclusion

In this work, we have developed a framework for tooth morphometry using quasi-conformal theory. Landmark-matching Teichmüller maps are first used for finding a 1-1 correspondence and the Teichmüller distance between tooth surfaces. Then, a quasi-conformal statistical shape analysis model based on the Teichmüller distance and curvature differences is developed for building a classification scheme. We have deployed our method on a dataset of Australian upper second premolars. Our method achieves better classification accuracy with respect to both ancestry and gender when compared to the existing methods. Moreover, the optimal parameters and statistically significant regions obtained by our model for the classifications reveal the shape difference between teeth from different groups. Future studies could incorporate blinded assessment to further assess the classification accuracy of this method. Nonetheless, this study highlights the promising application of quasi-conformal theory for shape analysis and group discrimination. In terms of the landmarking scheme, the current method is constrained by strict landmarking protocols, such as landmark correspondence and the presence of identifiable landmarks with associated low error rates. Therefore, the extension of the method for landmark-free quasi-conformal morphometry would be worth exploring.

For future work, we plan to perform a more comprehensive shape analysis on dentition using our proposed method. Besides human teeth, it is also possible for us to use our method for comparing the geometry of teeth of different mammals, and to compute Teichmüller mappings between specimens at different stages of tooth wear, which will enable us to capture the major shape difference between teeth at different wear level. We also plan to apply the framework for the study of other human organs.

Declaration of Competing Interest

None.

Acknowledgment

Gary P. T. Choi was supported by the Croucher Foundation, the Harvard Quantitative Biology Initiative and the NSF-Simons Center for Mathematical and Statistical Analysis of Biology at Harvard (Award number: #1764269). Lok Ming Lui was supported by HKRGC GRF (Project ID: 14303414).

References

[1] S. Loncaric, A survey of shape analysis techniques, Pattern Recognit. 31 (8) (1998) 983–1001.
[2] L.F.D. Costa, R.M. Cesar Jr, Shape Analysis and Classification: Theory and Practice, CRC Press, Inc., 2000.
[3] R.S. Ledley, L.B. Lusted, Reasoning foundations of medical diagnosis, Science 130 (3366) (1959) 9–21.
[4] R.S. Ledley, Digital electronic computers in biomedical science, Science 130 (3384) (1959) 1225–1234.
[5] R.S. Ledley, High-speed automatic analysis of biomedical pictures, Science 146 (3641) (1964) 216–223.
[6] R.A. Guler, S. Tari, G. Unal, Landmarks inside the shape: shape matching using image descriptors, Pattern Recognit. 49 (2016) 79–88.
[7] J. Gao, A.N. Evans, Expression robust 3d face landmarking using thresholded surface normals, Pattern Recognit. 78 (2018) 120–132.
[8] S. Huzurbazar, D. Kuang, L. Lee, Landmark-based algorithms for group average and pattern recognition, Pattern Recognit. 86 (2019) 172–187.
[9] F. Bookstein, Morphometric Tools for Landmark Data: Geometry and Biology, Cambridge University Press, Cambridge, 1991.
[10] J.C. Gower, Generalized procrustes analysis, Psychometrika 40 (1975) 33–51.
[11] F.L. Bookstein, Principal warps: thin-plate splines and the decomposition of deformations, IEEE Trans. Pattern Anal. Mach. Intell. 11 (1989) 567–585.
[12] P.T. Choi, K.C. Lam, L.M. Lui, FLASH: fast landmark aligned spherical harmonic parameterization for genus-0 closed brain surfaces, SIAM J. Imaging Sci. 8 (1) (2015) 67–94.
[13] L.M. Lui, T.W. Wong, P. Thompson, T. Chan, X. Gu, S.T. Yau, Shape-based diffeomorphic registration on hippocampal surfaces using Beltrami holomorphic flow, in: Med. Image Comput. Comput. Assist. Interv. (MICCAI), 2010, pp. 323–330.
[14] H.L. Chan, H. Li, L.M. Lui, Quasi-conformal statistical shape analysis of hippocampal surfaces for alzheimer disease analysis, Neurocomputing 175 (A) (2016) 177–187.
[15] C. Wen, D. Wang, L. Shi, W.C.W. Chu, J.C.Y. Cheng, L.M. Lui, Landmark constrained registration of high-genus surfaces applied to vestibular system morphometry, Comput. Med. Imaging Graph. 44 (2015) 1–12.
[16] G.P.T. Choi, Y. Chen, L.M. Lui, B. Chiu, Conformal mapping of carotid vessel wall and plaque thickness measured from 3d ultrasound images, Med. Biol. Eng. Comput. 55 (12) (2017) 2183–2195.
[17] G.W. Jones, L. Mahadevan, Planar morphometry, shear and optimal quasi-conformal mappings, Proc. R. Soc. A 469 (2153) (2013) 20120653.
[18] G.P.T. Choi, L. Mahadevan, Planar morphometrics using Teichmüller maps, Proc. R. Soc. A 474 (2217) (2018) 20170905.
[19] P.A. Kaestle, K.A. Horsburgh, Ancient DNA in anthropology: methods, applications, and ethics, Yearb. Phys. Anthropol. 45 (2002) 92–130.
[20] K.P. Mooder, et al., Matrilineal affinities and prehistoric Siberian mortuary practices: a case study from Neolithic Lake Baikal, J. Archaeol. Sci. 32 (2005) 619–634.
[21] L. Alvesalo, Human sex chromosomes in oral and craniofacial growth, Arch. Oral Biol. 54S (2009) S18–S24.
[22] G.T. Schwartz, M.C. Dean, Sexual dimorphism in modern human permanent teeth, Am. J. Phys. Anthropol. 128 (2005) 312–317.
[23] T. Hanihara, Morphological variation of major human populations based on nonmetric dental traits, Am. J. Phys. Anthropol. 136 (2008) 169–182.
[24] G. Polychronis, P. Christou, M. Mavragani, D.J. Halazonetis, Geometric morphometric 3d shape analysis and covariation of human mandibular and maxillary first molars, Am. J. Phys. Anthropol. 152 (2) (2013) 186–196.
[25] R. Yong, S. Ranjitkar, D. Lekkas, D. Halazonetis, A. Evans, A. Brook, G. Townsend, Three-dimensional (3d) geometric morphometric analysis of human premolars to assess sexual dimorphism and biological ancestry in australian populations, Am. J. Phys. Anthropol. 166 (2) (2018) 373–385.
[26] T. Brown, G.C. Townsend, S.K. Pinkerton, J.R. Rogers, Yuendumu: Legacy of a Longitudinal Growth Study in Central Australia, University of Adelaide Press, 2011.
[27] G.C. Townsend, S.K. Pinkerton, J.R. Rogers, M.R. Bockmann, T.E. Hughes, Twin Studies: Research in Genes, Teeth and Faces, University of Adelaide Press, 2015.
[28] T.W. Meng, G.P.-T. Choi, L.M. Lui, TEMPO: feature-endowed teichmüller extremal mappings of point clouds, SIAM J. Imaging Sci. 9 (4) (2016) 1922–1962.
[29] L.M. Lui, K.C. Lam, S.T. Yau, X. Gu, Teichmüller mapping (t-map) and its applications to landmark matching registration, SIAM J. Imaging Sci. 7 (1) (2014) 391–426.
[30] F. Gardiner, N. Lakic, Quasiconformal Teichmüller Theory, American Mathematics Society, 2000.
[31] E. Reich, Extremal quasi-conformal mappings of the disk, in: Handbook of Complex Analysis: Geometric Function Theory, Vol. 1,, Elsevier Science B.V., 2002, pp. 75–135.
[32] G.P.T. Choi, C.H. Rycroft, Density-equalizing maps for simply-connected open surfaces, SIAM J. Imaging Sci. 11 (12) (2018) 1134–1178.
[33] G.P.T. Choi, B. Chiu, C.H. Rycroft, Area-preserving mapping of 3D carotid ultrasound images using density-equalizing reference map, Preprint. arXiv:1812.03434.
[34] P.T. Choi, L.M. Lui, Fast disk conformal parameterization of simply-connected open surfaces, J. Sci. Comput. 65 (3) (2015) 1065–1090.
[35] G.P.-T. Choi, L.M. Lui, A linear formulation for disk conformal parameterization of simply-connected open surfaces, Adv. Comput. Math. 44 (1) (2018) 87–114.
[36] B. Leo, Bagging predictors, Mach. Learn. 24 (2) (1996) 123–140.
[37] https://scholar.harvard.edu/files/choi/files/tooth_morphometry.zip.
[38] S. Molnar, J.K. McKee, I.M. Molnar, Tooth wear rates among contemporary Australian Aborigines, J. Dent. Res. 62 (1983) 562–565.
[39] A. Gómez-Robles, et al., Geometric morphometric analysis of the crown morphology of the lower first premolar of hominins, with special attention to Pleistocene Homo, J. Hum. Evol. 55 (2008) 627–638.
[40] A. Gómez-Robles, et al., A geometric morphometric analysis of hominin upper premolars: shape variation and morphological integration, J. Hum. Evol. 61 (2011) 688–702.
[41] C. Loop, Smooth Subdivision Surfaces Based on Triangles, University of Utah, 1987 Master's thesis. M.S. Mathematics thesis.
[42] O. Colliot, et al., Discrimination between alzheimer disease, mild cognitive impairment, and normal aging by using automated segmentation of the hippocampus, Radiology 248 (1) (2008) 194–201.
[43] M. Chupin, et al., Fully automatic hippocampus segmentation and classification in Alzheimer's disease and mild cognitive impairment applied on data from ADNI, Hippocampus 19 (6) (2009) 579–587.

Gary P. T. Choi is with the John A. Paulson School of Engineering and Applied Sciences, Harvard University. His research interests include computational geometry, mathematical modeling and medical imaging.

Hei Long Chan is with the Department of Mathematics, The Chinese University of Hong Kong. His research interests include medical imaging, shape analysis and image segmentation.

Robin Yong is with the Adelaide Dental School, The University of Adelaide. His research interests include dental anthropology and 3D imaging.

Sarbin Ranjitkar is with the Adelaide Dental School, The University of Adelaide. His research interests include dental phenomics and craniofacial biology.

Alan Brook is with the Adelaide Dental School, The University of Adelaide. His research interests include medical anthropology and biological anthropology.

Grant Townsend is with the Adelaide Dental School, The University of Adelaide. His research interests include craniofacial biology and medical anthropology.

Ke Chen is with the Department of Mathematical Sciences, The University of Liverpool. His research interests include mathematical imaging and numerical linear algebra.

Lok Ming Lui is with the Department of Mathematics, The Chinese University of Hong Kong. His research interests include computational quasi-conformal geometry and medical imaging.